Guan M, Liang Q.

A two-dimensional hydro-morphological model for river hydraulics and morphology with vegetation.

***Environmental Modelling & Software* 2017, 88, 10-21**

A two-dimensional hydro-morphological model for river hydraulics and morphology with vegetation

Mingfu Guan[1*], Qiuhua Liang[2]

[1] Department of Geography, Loughborough University, LE11 3TU, UK

[2] School of Civil Engineering and Geosciences, Newcastle University, NE1 7RU, UK

[*] Corresponding to: mingfu.guan@hotmail.com

ABSTRACT: This work develops a two-dimensional (2D) hydro-morphological model which can be used to simulate river hydraulics and morphology under the condition of various vegetation covers. The model system consists of five modules, including a hydrodynamic model, a sediment transport model, a vegetation model, a bank failure model and a bed deformation model. The secondary flow effects are incorporated through additional dispersion terms. The core components of the model system solve the full shallow water equations; this is coupled with a non-equilibrium sediment transport model. The new integrated model system is validated against a number of laboratory-scale test cases and then applied to a natural river. The satisfactory simulation results confirm the model's capability in reproducing both stream hydraulics and channel morphological changes with vegetation. Several hypothetical simulations indicate that the model can be used not only to predict flooding and morphological evolution with vegetation, but also to assess river restoration involving vegetation.

KEYWORDS: vegetation effects; non-equilibrium sediment transport model; river hydraulics; morphological changes; shallow water equations

1. Introduction

Vegetation plays multiple roles in real-world river streams. For example, riparian vegetation can protect against bank erosion, and in-stream vegetation may significantly influence flow propagation, sediment movement and river morphology (Darby, 1999; Hickin, 1984; Hupp and Osterkamp, 1996; Keller and Swanson, 1979). Vegetation has been widely used for improving

stream corridor habitat and other ecological functions in many river restoration programmes. Understanding the multiple effects of vegetation is highly important in river management.

In the recent decades, the effects of vegetation on river flows have been extensively investigated through laboratory experiments (Armanini et al., 2010; Bennett et al., 2008; Gorrick and Rodríguez, 2012; Jordanova and James, 2003) and modelling (e.g. (Anderson et al., 2006; Crosato and Saleh, 2011; Gran and Paola, 2001; Jang and Shimizu, 2007; Li and Millar, 2011; Tal and Paola, 2007; Tal and Paola, 2010; Tsujimoto, 1999; Wu et al., 2005b)). These studies have clearly emphasised that vegetation affects flow hydraulics in various ways, and thereby plays a crucial role in river morphology and ecological diversity. However, the majority of the existing studies have been focused on the effects of vegetation on pure flow characteristics, with some considering the long-term flow-vegetation-sediment interaction in braided rivers. Research into the direct fluvial response to vegetation during flooding remains rare.

On the other hand, numerical models for hydro-geomorphological processes have been extensively developed (Guan et al., 2013; Guan et al., 2015b; Liang, 2010). When considering the importance of vegetation, hydro-morphological modelling should take into account the vegetation effects, particularly under conditions where vegetation may play a key role. Flow-sediment-vegetation interaction is a highly complex process where the three components may dynamically interact with each other. Few models have been reported to represent the whole physical process. The current study, therefore, presents a hydro-morphodynamic model with the inclusion of vegetation dynamics to fill this knowledge gap.

In reality, vegetation may or may not be fully submerged by river flows. For example, soft grass and plants are generally submerged during flooding seasons, while rigid vegetation, e.g. trees is usually emergent. In hydraulic and sediment transport modelling, the effects of vegetation is conventionally taken into account through increased resistant force and the Manning's equation has been the most widely-used approach to represent flow resistance (Green, 2005; Guan et al., 2013; Guan et al., 2015b; Liang, 2010; Sellin et al., 2003; Wu et al., 1999). The Manning's coefficient is usually estimated according to specific channel conditions and its accurate estimation requires abundant experience. However, this traditional way of representing flow

55 resistance is not appropriate for cases when rigid plants are present, e.g. flow through emergent
56 vegetation. In such flow scenarios, resistance is primarily exerted by the stem's drag throughout
57 the flow depth rather than by shear stress at the bed (James et al., 2004). A more appropriate
58 approach is to split channel resistance into several components and then estimate each one
59 separately (Cowan, 1956; Morin et al., 2000). Recently, some approaches have been
60 successively proposed to estimate the flow resistance for modelling flows over or through a
61 vegetated channel (Baptist et al., 2007; Vionnet et al., 2004). This study adopts the estimation
62 method of separating the total resistance into vegetation resistance and bed resistance. The
63 vegetation resistance is then treated as a *drag force* exerted by vegetation. This vegetation
64 resistance usually dominates flow resistance for the vegetated flows (Temple, 1986; Wu et al.,
65 1999) because the presence of emergent vegetation (such as trees), to a certain extent, narrows
66 the channel width, thereby altering flow properties.

67 This study aims to develop a depth-averaged 2D numerical model for river hydraulics and
68 morphology with vegetation effects, and to better understand the effects of vegetation on
69 changing river morphology through intensive numerical experiments. The numerical model is
70 built upon a layer-based 2D hydro-morphodynamic model (LHMM) (Guan et al., 2014; Guan et
71 al., 2015b) which has been validated by a variety of flood events. A vegetation module is
72 developed and incorporated in the model system to simulate vegetation effects. The model is
73 validated against several laboratory experiments before a real-world application is considered.

74

75 ## 2. Numerical Model (LHMM)

76 ### 2.1. Model framework

77 Shallow water based numerical models have been widely used for river flow modelling (Costabile
78 and Macchione, 2015; Guan et al., 2013; Hou et al.,2015; Vacondio et al, 2014). The layer-based
79 hydro-morphodynamic model (LHMM) that has been presented in previous work (Guan et al.,
80 2014, 2015a; Guan et al., 2015b) also solves the fully coupled shallow water equations (SWEs)
81 and the sediment transport formulation. Herein, a new vegetation model component is developed

and included in LHMM to consider the vegetation effects. The model system considers the mass and momentum exchange of non-cohesive sediment between bed and flow, and updates the hydraulic and sediment quantities per grid cell, per time step. Figure 1 shows the entire LHMM model framework, which includes four modules:

- ***Hydrodynamic module***: The depth-averaged 2D shallow water equations are solved to predict rapidly varying unsteady flows, taking into account the feedback from sediment and vegetation.
- ***Sediment transport module***: A non-uniform sediment transport model is developed to describe the transport of sediment particles.
- ***Vegetation module***: The external force exerted by vegetation on flow and sediment is parameterised.
- ***Bank failure module***: Is a model component to simulate lateral bank erosion or failure.
- ***Bed deformation module***: The bed elevation is updated after localised erosion and deposition of sediment.

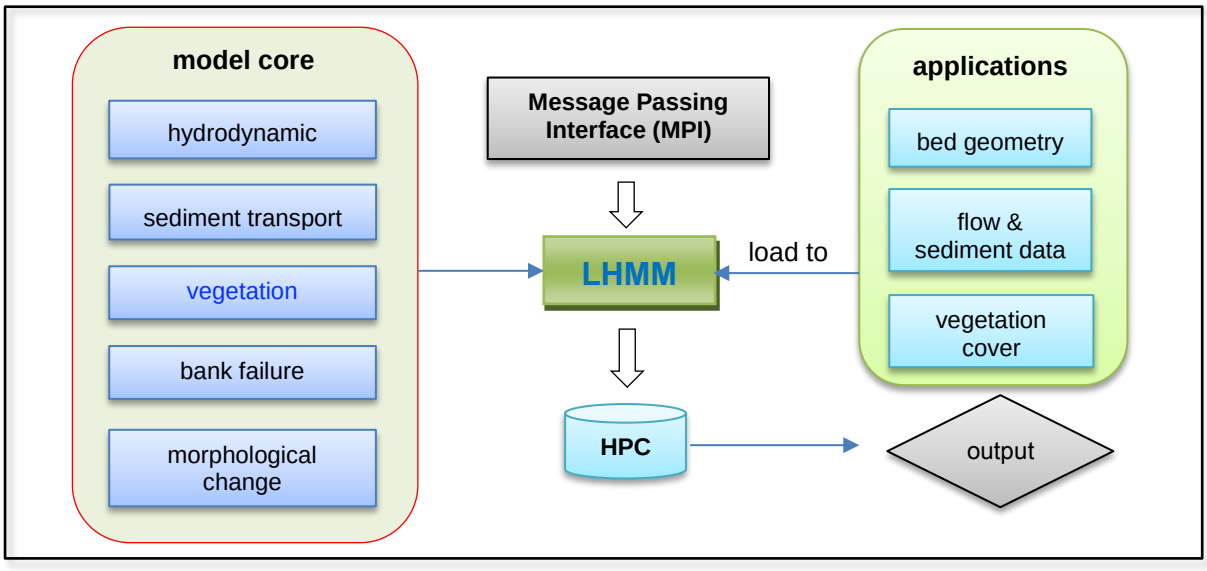

Figure 1. Model framework of LHMM

2.2. Hydrodynamic module

The hydrodynamic module solves the depth-averaged 2D shallow water equations, including the

effects of sediment and vegetation on flow dynamics. In a vector form, the governing equations can be expressed by

$$\frac{\partial \mathbf{U}}{\partial t}+\frac{\partial \mathbf{E}}{\partial x}+\frac{\partial \mathbf{F}}{\partial y}=\frac{\partial \tilde{\mathbf{E}}}{\partial x}+\frac{\partial \tilde{\mathbf{F}}}{\partial y}+\mathbf{S_o}+\mathbf{S_f}+\mathbf{S_v}+\mathbf{S_{fb}} \tag{1}$$

where

$$\mathbf{U}=\begin{bmatrix}\eta\\ hu\\ hv\end{bmatrix},\mathbf{E}=\begin{bmatrix}hu\\ hu^2+\frac{1}{2}gh^2\\ huv\end{bmatrix},\mathbf{F}=\begin{bmatrix}hv\\ huv\\ hv^2+\frac{1}{2}gh^2\end{bmatrix},\tilde{\mathbf{E}}=\begin{bmatrix}0\\ h(T_{xx}+D_{xx})\\ h(T_{xy}+D_{xy})\end{bmatrix},\tilde{\mathbf{F}}=\begin{bmatrix}0\\ h(T_{yx}+D_{yx})\\ h(T_{yy}+D_{yy})\end{bmatrix}$$

$$\mathbf{S_o}=\begin{pmatrix}0\\ -gh\frac{\partial z_b}{\partial x}\\ -gh\frac{\partial z_b}{\partial y}\end{pmatrix},\mathbf{S_f}=\begin{pmatrix}0\\ -ghS_{fx}\\ -ghS_{fy}\end{pmatrix},\mathbf{S_v}=\begin{pmatrix}0\\ -\frac{\tau_{vx}}{\rho_w}\\ -\frac{\tau_{vx}}{\rho_w}\end{pmatrix}$$

$$\mathbf{S_{fb}}=\begin{pmatrix}0\\ \frac{\Delta\rho u}{\rho}\frac{\partial z_b}{\partial t}[\alpha(1-p)-c]-\frac{\Delta\rho g h^2}{2\rho}\frac{\partial C}{\partial x}-S_a\\ \frac{\Delta\rho v}{\rho}\frac{\partial z_b}{\partial t}[\alpha(1-p)-c]-\frac{\Delta\rho g h^2}{2\rho}\frac{\partial C}{\partial y}-S_b\end{pmatrix} \tag{2}$$

where **U** is the vector of conserved variables; **E** and **F** are the flux vectors of the flow in the *x* and *y* directions respectively, $\tilde{\mathbf{E}}$ and $\tilde{\mathbf{F}}$ contain the turbulent and dispersion terms in the *x* and *y* directions, $\mathbf{S_o}$ and $\mathbf{S_f}$ are the vectors containing the bed slope terms and the frictional slope terms, $\mathbf{S_v}$ contains vegetation terms, and $\mathbf{S_{fb}}$ is the vector of flow-bed interaction terms. In these vector terms, h = flow depth, z_b = bed elevation, η = water surface elevation, u and v = the depth-averaged flow velocity components in the two Cartesian directions, T_{xx}, T_{xy}, T_{yx} and T_{yy} are the depth-averaged turbulent stresses, D_{xx}, D_{xy}, D_{yx} and D_{yy} are the dispersion terms due to the effect of secondary flow, p = sediment porosity, c = total volumetric sediment concentration, τ_{vx} and τ_{vy} are the vegetation shear stresses in the *x* and *y* directions; ρ_s and ρ_w denote the densities of sediment and water respectively, $\Delta\rho = \rho_s - \rho_w$, ρ = density of flow-sediment mixture, α = sediment-to-flow velocity ratio determined by

$$\alpha=\frac{u^*}{u}\frac{1.1(\theta/\theta_{cr})^{1.7}[1-\exp(-5\theta/\theta_{cr})]}{\sqrt{\theta_{cr}}} \tag{3}$$

where θ and θ_{cr} represent the real dimensionless bed shear stress, and the critical Shields parameter, u^* is shear velocity. S_a and S_b are the additional terms related to the velocity ratio defined by Guan et al. (2014)

$$S_a = \frac{\Delta\rho u}{\rho}(1-\alpha)[c\nabla\cdot(h\mathbf{V}) - (h\mathbf{V})\nabla\cdot\mathbf{C}]$$

$$S_b = \frac{\Delta\rho v}{\rho}(1-\alpha)[c\nabla\cdot(h\mathbf{V}) - (h\mathbf{V})\nabla\cdot\mathbf{C}] \quad (4)$$

where $\nabla = \vec{\imath}(\partial/\partial x) + \vec{j}(\partial/\partial y)$; **C** is the sediment concentration vector defined by $\mathbf{C} = c(\vec{\imath} + \vec{j})$; **V** is the velocity vector defined by $\mathbf{V} = u\vec{\imath} + v\vec{j}$.

The depth-averaged turbulent stresses are determined by the Boussinesq approximation which has been widely used in the literature (e.g. (Abad et al., 2008; Begnudelli et al., 2010; Wu, 2004)). This gives the Reynolds stresses as:

$$T_{xx} = -2(\nu_t + \nu)\frac{\partial u}{\partial x} \quad (5a)$$

$$T_{xy} = T_{yx} = -(\nu_t + \nu)\left(\frac{\partial u}{\partial x} + \frac{\partial v}{\partial x}\right) \quad (5b)$$

$$T_{yy} = -2(\nu_t + \nu)\frac{\partial v}{\partial x} \quad (5c)$$

where ν_t is the turbulence eddy viscosity and ν is the molecular viscosity, which can be ignored in environmental applications. Various approaches have been adopted to estimate the turbulence viscosity, e.g. assuming a constant eddy viscosity, an algebraic turbulence model ($\nu_t \sim hu^*$), as well as the k - ε turbulence model. In this study, the eddy viscosity is estimated by $\nu_t = \beta h u^*$ with β = 0.5. The dispersion terms are generally delivered from the difference of the depth-averaged velocity and the vertical varying velocity as follows:

$$D_{xx} = \frac{1}{h}\int_{z_0}^{z_0+h}[u(z)-u]^2\,dz \quad (6a)$$

$$D_{xy} = D_{yx} = \frac{1}{h}\int_{z_0}^{z_0+h}[u(z)-u]\,[v(z)-v]\,dz \quad (6b)$$

$$D_{yy} = \frac{1}{h}\int_{z_0}^{z_0+h}[v(z)-v]^2\,dz \quad (6c)$$

where z_0 is the zero velocity level; $u(z)$ and $v(z)$ represents the x and y components of the vertically varying velocity respectively. A number of approaches have been proposed to calculate the vertical varying velocity both in the streamwise and transverse directions (e.g. (De Vriend, 1977; Guymer, 1998; Odgaard, 1986; Wu et al., 2005a)). The Odgaard's equation, based on the

linear transverse velocity profiles over the depth, is employed in this work because of its robustness and simplicity. The longitudinal and transverse velocities are given as (Odgaard, 1986):

$$u_l(z) = U\frac{m+1}{m}\xi^{1/m} \tag{7a}$$

$$u_t(z) = 2v_s\left(\xi - \frac{1}{2}\right),\ v_s = U\frac{2m+1}{2\kappa^2 m}\frac{h}{r_c} \tag{7b}$$

where $u_l(z)$ and $u_t(z)$ are the longitudinal and transverse velocity components in the streamline coordinates, respectively; U is the depth-averaged longitudinal velocity; $m = \kappa C/g^{0.5}$ with κ = 0.41 being the von Karman's constant; v_s represents the transverse velocity at the free surface; $\xi = (z-z_0)/h$ is the dimensionless distance from the bed; r_c is the radius of curvature. Following the study (Begnudelli et al., 2010), integration of Eqs. (6) using the velocity profiles Eq. (7) yields:

$$D_{ll} = \frac{U^2}{m(2+m)};\ D_{lt} = D_{tl} = \frac{Uv_s}{1+2m};\ D_{tt} = \frac{v_s^2}{3} \tag{8}$$

Defining the angle of the depth-averaged velocity vector measured counter-clockwise from the x direction as φ, the dispersion terms in the curvilinear coordinates can then be converted to the Cartesian coordinate system by:

$$\begin{bmatrix} D_{xx} & D_{xy} \\ D_{yx} & D_{yy} \end{bmatrix} = \mathbf{M}(\varphi)\begin{bmatrix} D_{ll} & D_{lt} \\ D_{tl} & D_{tt} \end{bmatrix}\mathbf{M}^{\boldsymbol{T}}(\varphi)$$

where $\mathbf{M}(\varphi) = \begin{bmatrix} \cos\varphi & -\sin\varphi \\ \sin\varphi & \cos\varphi \end{bmatrix}$, so this leads to:

$$D_{xx} = D_{ll}\cos^2\varphi - 2D_{lt}\sin\varphi\cos\varphi + D_{tt}\sin^2\varphi \tag{9a}$$

$$D_{xy} = (D_{ll} - D_{tt})\sin\varphi\cos\varphi + D_{lt}(\cos^2\varphi - \sin^2\varphi) \tag{9b}$$

$$D_{yy} = D_{ll}\sin^2\varphi + 2D_{lt}\sin\varphi\cos\varphi + D_{tt}\cos^2\varphi \tag{9c}$$

Eqs.(9) accounts for the effect of secondary flow which is included in the hydrodynamic governing equations.

2.3. Sediment transport module

The governing equation of the ith size sediment class is written according to the velocity ratio α

by

$$\frac{\partial hc_i}{\partial t} + \frac{\alpha \partial huc_i}{\partial x} + \frac{\alpha \partial hvc_i}{\partial y} = -\frac{\alpha(q_{bi} - F_i q_{b*i})}{L_i} \tag{10}$$

where c_i = depth-averaged volumetric bedload concentration of the ith size class; $q_{bi} = h\overline{U}c_i$ = real sediment transport rate of the i^{th} fraction; $\overline{U} = \sqrt{u^2 + v^2}$ is the depth-averaged velocity; q_{b*i} = sediment transport capacity of the i^{th} fraction; F_i represents the proportion of i^{th} grain-size fraction in the total moving sediment and is updated at each time step using the approach presented by Wu (2004); L_i = non-equilibrium adaptation length of sediment transport of the i^{th} fraction which is estimated by

$$L_i = \frac{h\sqrt{u^2 + v^2}}{\gamma \omega_{f,i}} \text{ with } \gamma = \min\left(\alpha \frac{h}{h_b}, \frac{1-p}{c}\right) \tag{11}$$

where h_b is the thickness of a sheet flow layer; ω_{fi} is the effective setting velocity of a sediment particle which is determined by the formula proposed by Soulsby (1997):

$$\omega_{fi} = \frac{\nu}{d_i}\left(\sqrt{10.36^2 + 1.049(1-c)^{4.7} d_*^3} - 10.36\right) \tag{12}$$

where $d_* = d_i[(s\text{-}1)g/\nu^2]^{1/3}$ is the dimensionless particle diameter.

The bed load is estimated using the Meyer-Peter & Müller equation (Meyer-Peter and Müller, 1948)

$$q_{b*i} = 8\left(\theta_i - \theta_{cr,i}\right)^{1.5} \sqrt{(s-1)g d_i^3} \tag{13}$$

where $\theta_{cr,i}$ is the critical dimensionless bed shear stress of the i^{th} fraction; θ is the dimensionless bed shear stress; $s = (\rho_s/\rho_w - 1)$ is the special gravity of sediment.

2.4. Vegetation module

In the current model framework, vegetation is catalogued into two types according to the stiffness and submerged extent: (i) submerged flexible vegetation, such as grass; (ii) submerged or emergent plants with rigid or hard stems (rigid vegetation). The vertical distribution of flow velocity in the two types of vegetation is sketched in Figure 2. In case of submerged flexible

vegetation, the existence of vegetation elevates the total resistance, thereby reducing the flow velocity. For the flow over submerged rigid plants, the velocity in the lower layer of the plants is obviously decreased because of the resulting drag force and the effect caused by narrowed channel width. The decreased velocity can reduce bed shear stress, and subsequently weaken the sediment transport capability of the flow. In the case of emergent rigid plants, the main feature of velocity distribution is similar to that in Figure 2(a), but the magnitude of velocity may be significantly affected by plants and hence different, as shown in Figure 2(c). When considering vegetation in flow modelling, a common approach is to treat vegetation as rigid cylinders with the same diameter, same species and same spacing (Bennett et al., 2008; Choi and Kang, 2006; Wu et al., 2005b).

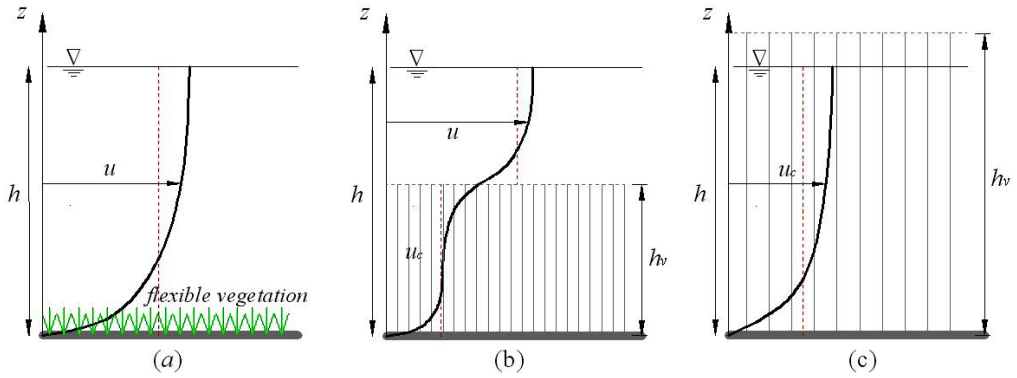

Figure 2 Flow velocity distribution with vegetation: (*a*) flow over submerged flexible vegetation; (b) flow over submerged rigid plants; (c) flow through emergent rigid plants

2.4.1. Bed shear stress effective to sediment transport

In Eq. (2), the shear stresses related to grain roughness and vegetation roughness are treated separately. In other words, the flow resistance is divided to two parts to obtain the appropriate Manning's *n*, i.e. the resistance exerted by the bed and the resistance exerted by the vegetation. This method has been adopted by many other studies (Crosato and Saleh, 2011; Li and Millar, 2011) because it can not only reflect the decreasing of bed shear stress which reduces the sediment transport capacity in the vegetation layer, but also elucidate the increasing of total resistance which reduces flow velocity within and above plants. The final expression of the Manning coefficient is given by

213 $$n = \sqrt{n_1^2 + n_2^2} \tag{14}$$

214 where n_1 is the Manning's coefficient related to grain roughness; n_2 is the Manning's coefficient
215 associated with the flexible vegetation roughness. Whilst for the rigid plants, the vegetation shear
216 stress τ_b is calculated by formula below

217 $$\boldsymbol{\tau_b} = \frac{\rho_w g n_1^2 \mathbf{U}_c |\mathbf{U}_c|}{h^{1/3}} \tag{15}$$

218 The corresponding dimensionless bed shear stress is calculated by

219 $$\theta_i = \frac{|\boldsymbol{\tau_b}|}{\rho_w g (s-1) d_i} = \frac{n_1^2 |\mathbf{U}_c|^2}{(s-1) d_i h^{1/3}} \tag{16}$$

220 where $\mathbf{U}_c$ is the vector of depth-averaged flow velocity in the vegetation layer; for emergent
221 vegetation, it is equal to the depth-averaged flow velocity $\mathbf{U}$; $|\mathbf{U}_c|$ is the magnitude of $\mathbf{U}_c$
222 determined using the Stone and Shen's equation (Stone and Shen, 2002).

223 $$\mathbf{U}_c = \delta \mathbf{U} \sqrt{\left(\frac{h_v}{h}\right)} \tag{17}$$

224 in which, δ is a coefficient approximately equal to 1.0; h_v represents the height of rigid plants.
225 When calculating the sediment transport rate, the velocity in the vegetation layer will be used
226 instead of the depth-averaged flow velocity.

227 ***2.4.2. Parameterisation of vegetation shear stress***

228 In the current model system, the vegetation is parameterised according to the classification of
229 vegetation. The effects of flexible vegetation are represented through the shear stress related to
230 the vegetation roughness by

231 $$\boldsymbol{\tau_v} = \frac{\rho_w g n_2^2 \mathbf{U} |\mathbf{U}|}{h^{1/3}} \tag{18}$$

232 For rigid plants, individual elements of plants are identified as disperse obstacles with drag
233 forces, but this will be spatially averaged to give a shear stress per unit volume of water as

234 $$\boldsymbol{\tau}_v = \frac{1}{2} \rho_w \lambda C_D h |\mathbf{U}_c| \mathbf{U}_c \tag{19}$$

where C_D represents the drag coefficient of vegetation elements; λ denotes the projected area of vegetation elements per unit volume of water, given by

$$\lambda = \frac{4\alpha_v V_d}{\pi D_v} \tag{20}$$

where α_v is a shape factor, V_d represents the vegetation density in vegetated zones (%), D_v is the diameter of the plant stems; l and w are the length and width of vegetated channel, respectively. Therefore, the vegetation shear stress τ_{vx} and τ_{vy} exerted by rigid plants in Eq. (1) are calculated by

$$\tau_{vx} = \frac{1}{2}\rho_w \lambda C_D h u_c \sqrt{u_c^2 + v_c^2} \tag{21a}$$

$$\tau_{vy} = \frac{1}{2}\rho_w \lambda C_D h v_c \sqrt{u_c^2 + v_c^2} \tag{21b}$$

where u_c and v_c are the depth-averaged flow velocity in the vegetation layer in the x and y directions. Previous studies (Alonso, 2004; Garcia et al., 2004; Lopez and Garcia, 2001) have demonstrated that the drag coefficient C_D is usually in the range of 0.8 and 3.5, and typically varies from 1 to 1.5 (Garcia et al., 2004).

2.5. Bed deformation module

The erosion and deposition process is calculated per grid cell at each time step to update the new bed elevation based on the results from the previous hydrodynamic model, sediment transport model and vegetation model. The bed deformation is calculated by

$$\frac{\partial z_b}{\partial t} = \frac{1}{1-p}\sum_{i=1}^{N}\left[\frac{(q_{bi} - F_i q_{b*i})}{L_i}\right] \tag{22}$$

where the values of the parameters in the right hand side are calculated according to the equations already explained in previous sections.

2.6. Lateral bank erosion

Bank erosion is one of the key morphological processes affecting the evolution of river channels, particularly river banks. In reality, bank failure is a complex process which is closely related to many physical factors, such as vegetation and soil properties. Since this study aims to

investigate the physical process of flow and sediment transport in the presence of vegetation, we adopt a simplified bank failure model to represent the lateral bank erosion. The principle of the adopted method is that if the bank slope becomes steeper than the critical angle of failure, the bank will fail to form a new bedform with a slope approximately equal to the critical angle of repose. The bank failure process is simulated according to this principle, while maintaining mass conservation of sediment material. Different values are used for 1) the critical angles that initiate bank failure, and 2) the reformation bed angles above and below the water. Here, the wet and dry conditions are defined according to the simulated water depth at each time step. The bank failure model is described in detail in Guan et al. (2014).

2.7. Model solution procedure

The model's governing equations (Eqs.1,10, 22) are solved numerically by a well-balanced Godunov-type finite volume method (FVM) on Cartesian grids and details can be found in previous publications (Guan et al., 2013, 2014). As shown in Figure 3, the computation procedure at each time step consists of the following steps:

(1) Load the data files (hydraulics, sediment, vegetation cover) to the model;
(2) Calculate shear stresses exerted by the bed (Eq.15) and the vegetation (Eq.18, 19);
(3) Calculate sediment transport rate and capacity in each cell;
(4) Solve the coupled governing equations (Eqs.1,10) to update hydraulic variables and sediment concentration to the new time step;
(5) Update the bed elevation using Eq.(22);
(6) Activate the bank failure module if bank erosion occurs;
(7) Update the changes in river morphology;
(8) Return to step (1) and start the calculation at a new time step
(9) Repeat step (1) to (8) until the end of the simulation.

As the numerical scheme is explicit, the numerical stability of the model system is controlled by the CFL condition, which may be used to determine the time step Δt at each time step using the following equation

286 $$\Delta t = CFL \min\left(\min \frac{dx_i}{|u_i| + \sqrt{gh_i}}, \min \frac{dy_j}{|v_j| + \sqrt{gh_j}}\right) \quad (25)$$

287 The Courant number 0 < *CFL*< 1.0 is implemented for flow calculation, taking into account
288 additional conditions for sediment transport and bed change.

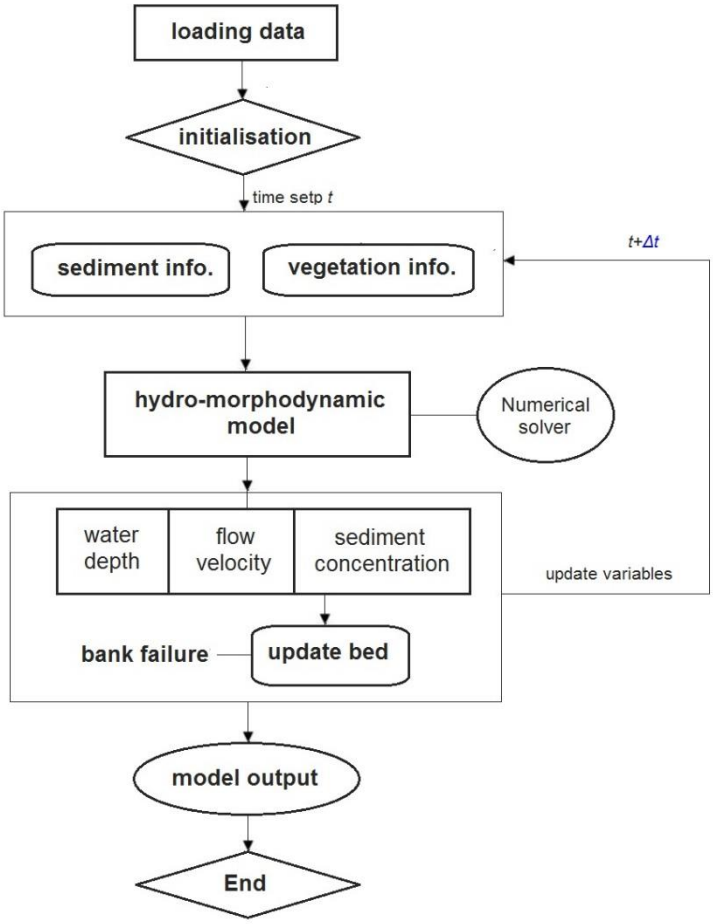

289

290 Figure 3 Workflow diagram of LHMM model core

291 ## 3. Results and Discussion

292 ### 3.1. Model validation

293 In this section, the new hydraulics-morphology-vegetation modelling system is validated against
294 a number of laboratory-scale test cases, including steady flow over a compound channel with a
295 fixed bed (Pasche and Rouvé, 1985) and steady flow over a compound channel with a movable
296 bed (Bennett et al., 2008).

3.1.1. Flow over a compound channel with a vegetated floodplain

The experiments conducted by Pasche and Rouvé (1985) are first considered to verify the capability of the model in accurately simulating shallow flow hydrodynamics in the presence of vegetation. The experiment was carried out in a 25.5 m x 1.0 m compound channel with a floodplain covered by vegetation. The cross-section of the channel is shown in Figure 4. Circular wooden cylinders with a uniform diameter of 0.012 m are used to represent the vegetation in the floodplain. Two experimental cases are considered in this work: Case 1 has a vegetative density of 0.0126 and bed slop of 0.001; Case 2 has a vegetative density of 0.0253, and bed slope of 0.0005. For both cases, the initial water depth is 0.2 m in the main channel and 0.076 m in the floodplain and an inflow discharge of 0.0345 m^3/s is fed from the upstream boundary to drive the steady flow.

During the simulations, the key coefficients for the channel and floodplain are specified as follows: for the simple cylindrical vegetation, shape factor = 1.0; Manning's n = 0.01; drag coefficient C_d = 1.5. The experimental flume is discretised using a mesh with 255 × 100 uniform cells of 0.1 m × 0.01 m. Figure 5 presents the simulations results for both of the experiments, where the modelled cross-section velocity profiles are compared satisfactorily with the laboratory measurements. The velocity in the vegetated zone is significantly smaller than that in the main channel, and the flow velocity in the vegetated floodplain decreases with higher vegetated density (Figure 5(b)). Successful simulation of this laboratory test demonstrates that the proposed model is capable of accurately simulating shallow flow hydrodynamics in the presence of vegetation.

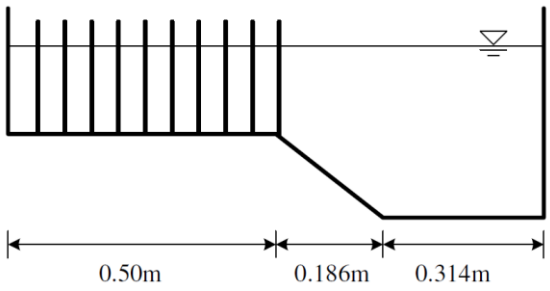

Figure 4. Cross-section of the flume used in the experiment of Pasche and Rouve (1995).

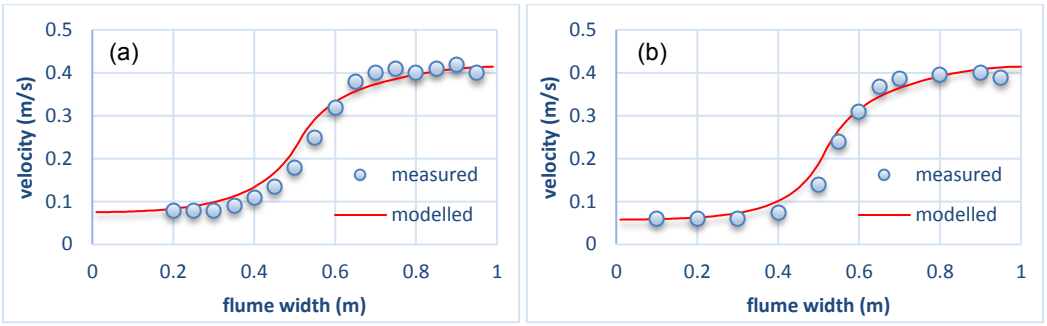

Figure 5. Measured and modelled velocity profiles for the two experiments with different vegetation density: (a) Case 1 (vegetative density of 0.0126); (b) Case 2 (vegetative density of 0.0253).

3.1.2. Fluvial response to in-stream woody vegetation

A series of experiments have been conducted in the hydraulic laboratory of Buffalo University to examine in detail the response of a stream corridor to woody vegetation of various configurations (e.g. (Bennett et al., 2002; Bennett et al., 2008)). These experiments provide further valuable datasets for the validation of the current hydraulics-morphology-vegetation modelling system. The experiments reported in Bennett et al. (2008) are considered herein to verify model capability in predicting alluvial response to riparian vegetation.

The experiments were performed in a flume which is 10 m long, 0.63 m wide and 0.61 m deep. The channel was first filled with a 0.5 m thick pre-wetting layer of sands with a uniform grain diameter of 0.8 mm. A 5 m long trapezoidal channel was cut out from the sand layer using an aluminium plate mounted on a movable carriage above the flume. The trapezoidal sand channel had a top width of 0.312 m, a bottom width of 0.1 m and a slide slope of 33. An adjustable weir was installed to control the flow depth, which was initially 0.069 m in the main channel, A constant inflow (Q = 0.0033 m^3/s) was imposed from the upstream boundary of the channel. In the experiments, the channel was covered by three vegetation zones where emergent, rigid wooden dowels with a diameter of 5 mm were planted. Two zones were on the left and one on the right, with each spaced 1.5 m apart. Vegetation zones of different shapes were used in the experiments, two of which are modelled in this work: (1) 0.5 m × 0.25 m rectangle; (2) 0.5 m diameter semicircle. For both cases, the vegetation density is chosen to be 0.0294.

Both simulations last for 6600s, the flume is discretised by a mesh of 0.05 m × 0.01 m uniform cells. The experiment indicates that no sediment transport occurs in the absence of vegetation.

344 To ensure this, the manning's *n* is set to 0.028. The shape factor and drag coefficient are
345 respectively set to 1.2 and 2.0.

346 Figure 6 demonstrates the modelled and measured changes in channel bed elevation in the
347 presence of the rectangular vegetation zone. It is clearly shown that the modelled bed changes
348 are generally in good agreement with observations, in terms of both the pattern and magnitude of
349 net erosion and deposition. Around the rectangular vegetation zone, the model predicts two
350 erosion patches that closely agreed with the measurements, one in the opposite side of the
351 vegetation zone and another in the upstream bank area. However, although the deposition in the
352 mid-channel region is correctly modelled, the deposition depth upstream of the vegetation zone
353 is predicted to be smaller than the observed results; additionally the model slightly overestimates
354 the mid-channel deposition downstream of the vegetation zone. As a whole, the current model
355 simulates reasonably well the alluvial process in response to riparian vegetation in this case,
356 considering the various uncertainties existing in sediment transport models.

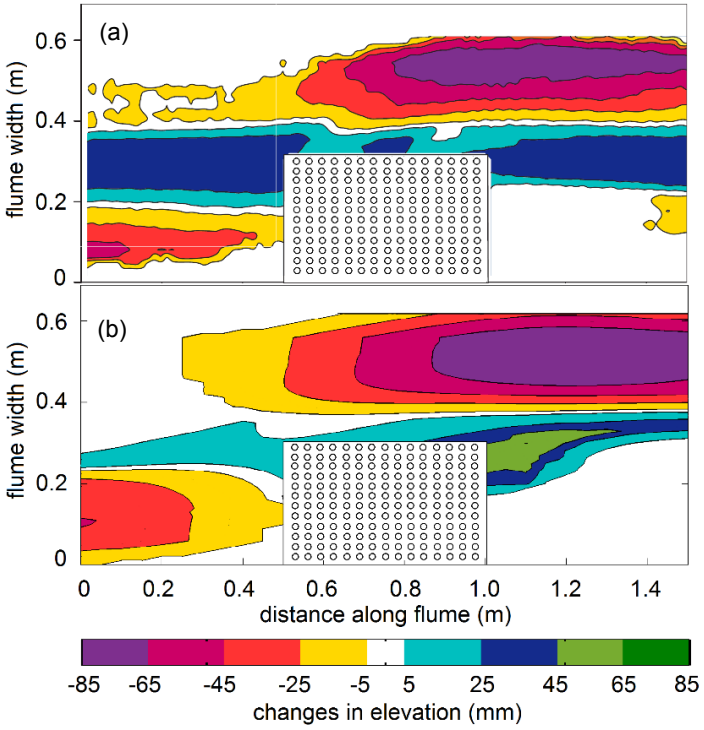

357

358 Figure 6. Contour plots of changes in channel bed elevation in the presence of rectangular vegetation: (a)
359 observed result; (b) simulation result.

360 With identical model parameters, the model simulates the case presented with a semicircle
361 vegetation zone. The predicted bed changes are shown in Figure 7, in comparison with the

362 laboratory measurement. The current model again predicts the general pattern of the channel
363 erosion and deposition around the vegetation zone reasonably well. As with the rectangular
364 vegetation patch case, discrepancies between the modelled and measured results are observed
365 in the mid-channel deposition zone. Further comparison is made in Figure 8 by plotting the
366 measured and predicted bed profiles at three cross-sections which are located at the front (- 0.5
367 m) (CS1), the middle (0 m) (CS2) and the back (0.5 m) (CS3) of the semicircle vegetation zone.
368 Clearly, the predicted bed profiles agree with the measurements reasonably well. Particularly,
369 erosion takes place at the left bank while deposition is found in the mid-channel at CS1; at both
370 CS2 and CS3, erosion happens at the right bank which is accurately predicted, but the model
371 slightly overestimates the deposition at CS2. Overall, successful reproduction of these two tests
372 confirms that the present model is capable of simulating morphological changes in the presence
373 of vegetation. From the results, it may be concluded that riparian vegetation has a significant
374 effect on the morphological change of the river corridor.

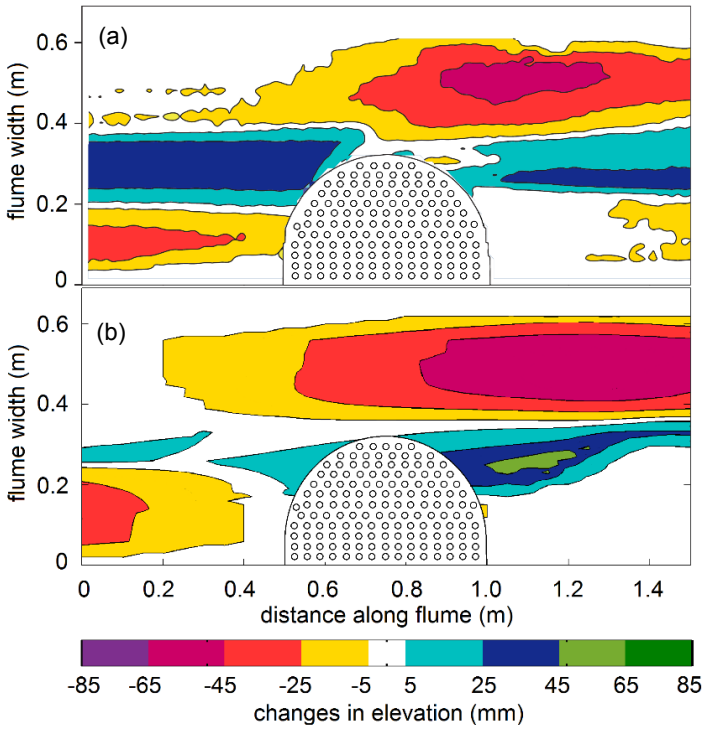

375

376 Figure 7. Contour plots of changes in channel bed elevation in the presence of semicircle vegetation: (a)
377 observed result; (b) modelled result.

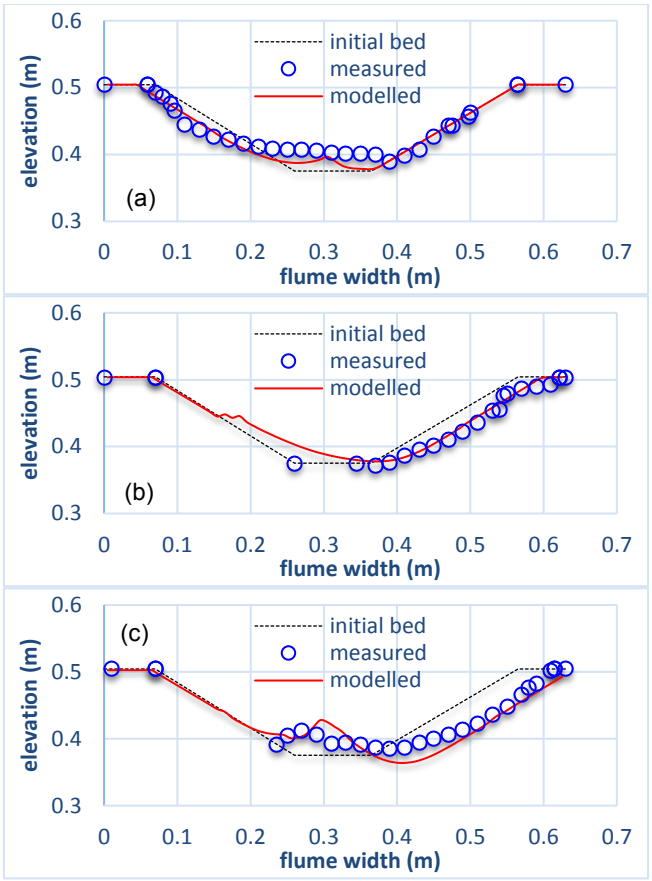

Figure 8. Modelled and measured bed profiles at (a) the front (-0.5 m), (b) the middle (0 m) and (c) the back (+0.5 m) of the vegetation zone

3.2. Channel pattern adjustment to riparian vegetation

Based on the validation cases presented above, numerical experiments with different vegetation covers are designed to further explore the effects of riparian vegetation on channel pattern adjustment at a wider context. The simulations are parameterised with the same main channel shape, the same streamwise bed slope, and the same sediment material as the experimental cases considered in 3.1.2. But the length of the erodible bed is extended from 5 m to 9 m, and the floodplain width from 0.07 m to 0.37 m at both sides in order to investigate the lateral bank erosion. Five vegetation zones are placed at both sides of the main channel. The location of these five vegetation zones and the initial channel are illustrated in Figure 9(a). Each vegetation patch has the same vegetation density, plant diameter and drag coefficient.

Figure 9 presents the snapshots of the simulation results at different output times, demonstrating changes in channel pattern in response to the five emergent, woody vegetation zones. Overall,

395 the presence of vegetation patches forces the channel to become meandering after initially being
396 straight. The presence of vegetation changes the flow field by increasing velocity at the opposite
397 size of the vegetation zones, but reducing the velocity within the vegetation zones. Accordingly,
398 the modified flow field leads to the deformation of the channel corridor. Figure 10 further shows
399 the erosion and deposition patterns in the channel at different output times. It is clear that the
400 eroding process dominates channel changes at the opposite sides of the vegetation zones and
401 that erosion becomes more severe and tends to be in a steady state over the time. Meanwhile,
402 deposition occurs around the vegetation, which can be attributed to two main causes: (1) the
403 deposition in front of the vegetation zone is caused by blockage effects of the vegetation; (2)
404 since the initial bank slope is approximately equal to the angle of repose of the sediment, bed
405 erosion initiates the repose and retreatment of the lateral bank which subsequently leads to
406 some deposition at the bank toe.

407 From the numerical experiments, the downstream channel is observed to be more intensively
408 meandering. This is because the change in velocity at the downstream is more significant due to
409 the presence of vegetation upstream. This indicates that vegetation can pose consistent and
410 cumulative effects on the morphological changes to a river corridor. From the simulation results,
411 it is clearly seen that the thalweg of the stream corridor is gradually changed from a straight line
412 to a meandering curve with a wavelength equal to the interval of vegetation zones. Furthermore
413 the channel is significantly widened, particularly at the downstream, which is consistent with the
414 forms of natural river systems.

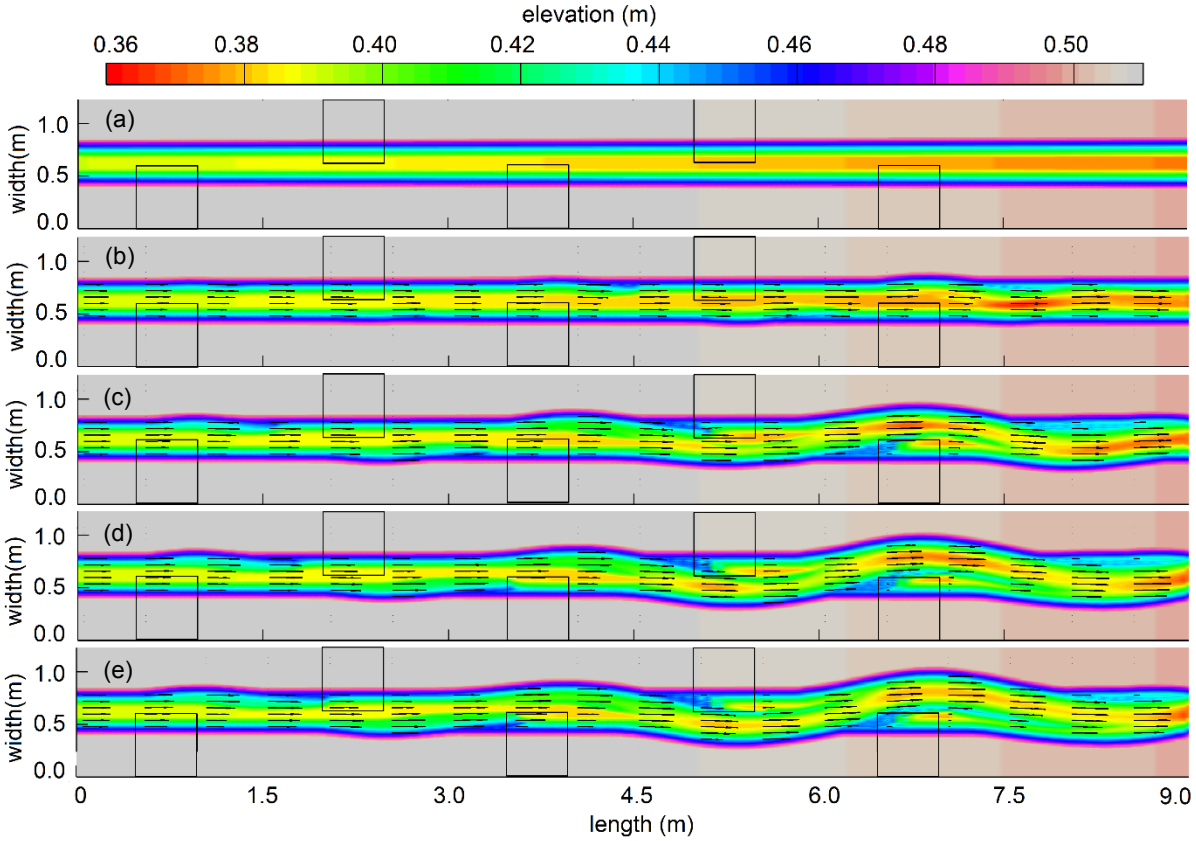

415

416 Figure 9. Channel pattern adjustment in response to multiple vegetation patches along a straight river corridor.

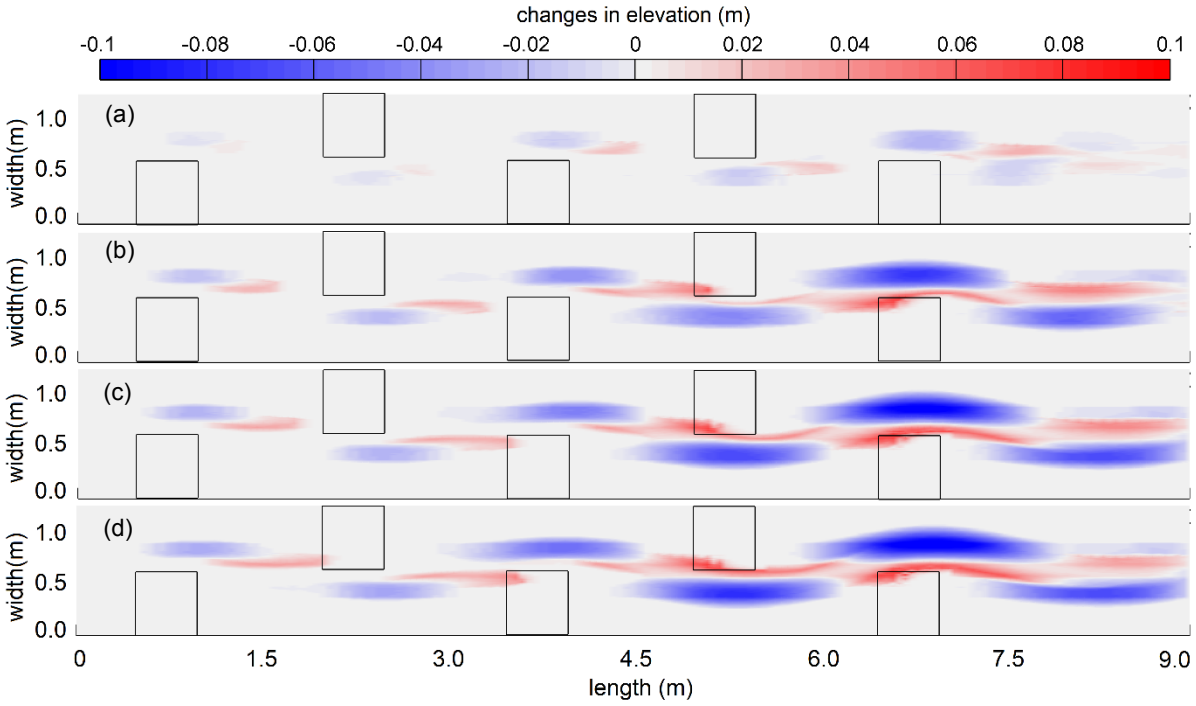

417

418 Figure 10. Erosion and deposition of the channel in response to the vegetation against time.

419 The alluvial response to the vegetation zone is more remarkable under the condition of higher

420 inflow discharge, as demonstrated in Figure 11. Compared with the lower inflow (Q_{in}), the higher

421 inflow discharge ($1.5Q_{in}$) induces more severe lateral bank erosion, particularly near the
422 upstream vegetation zones. Both bank erosion width and size are much larger near the first four
423 vegetation zones for the $1.5Q_{in}$ inflow. However, the difference becomes smaller after the fifth
424 vegetation patch.

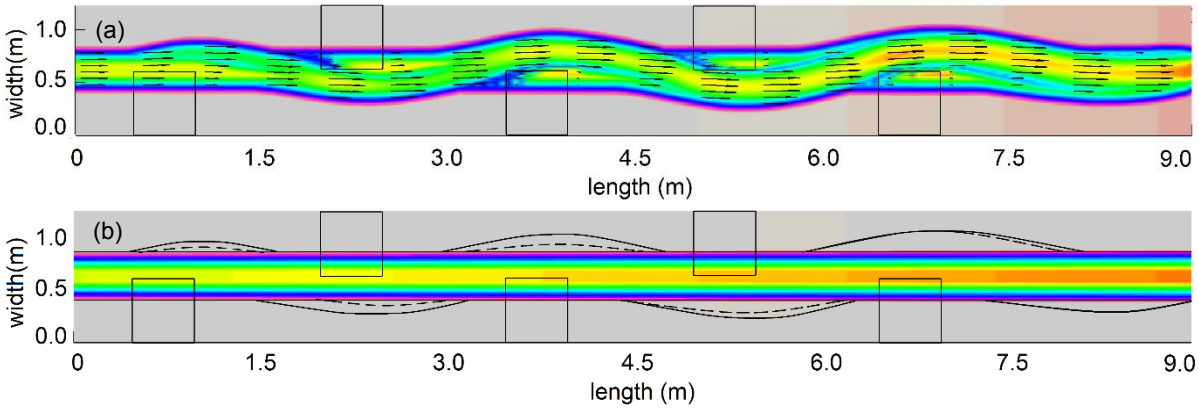

425
426

427 Figure 11. Adjusted channel patterns corresponding to different inflow conditions: (a) $1.5Q_{in}$; (b) comparison of
428 adjusted bank lines for two different flow conditions, i.e. Q_{in} and $1.5Q_{in}$.

429 The above numerical experiments are conducted under the condition that the five vegetation
430 zones are separated by equal distance. The meandering response of the channel form can be
431 easily understood due to the location of vegetation zones. Herein, another numerical experiment
432 with a single vegetation patch is designed and conducted. Figure 12 presents the resulting
433 alluvial process in response to the single vegetation zone. The simulation results indicate that a
434 single vegetation zone can also trigger the formation of a meandering channel with the maximum
435 bank curvature located behind the vegetation zone. Channel widening occurs at the opposite
436 side of the vegetation zone and the curve length becomes larger over time (line 1 shows the end
437 of the first curve). The changes in velocity field around the vegetation lead to an oscillation in
438 downstream velocity, causing the formation of a second curve after the vegetation; similarly, the
439 curve width increases over time (as shown in line 2). Moreover, lateral bank erosion occurs along
440 the whole downstream channel behind the vegetation zone. Although meandering occurs, it has
441 a relative smaller intensity due to the weaker effects on flow caused by a single vegetation patch.
442 Additionally a bar (bar 1 in Figure 12) is created at the location of the vegetation zone; following
443 the meandering curve, a larger bar (bar 2) is formed due to the effects of upstream vegetation on
444 channel erosion and deposition; the third and fourth bars appear and develop gradually along the

channel. It can be expected that the erosion and deposition patterns of a stream corridor become much more diverse and complicated over time if vegetation zones become more irregular.

The above hypothetical numerical experiments confirm that riparian and in-stream vegetation coves have a significant impact on local channel hydraulics and thereby stream morphology. The results imply that vegetation plays a key role in pushing flow towards the opposite side and hence protecting the localised bed; however it may cause severe erosion at the opposite side of the channel. The vegetation effects are persistent along the channel and further downstream, which may have a positive impact on and enhance stream biodiversity. This suggests that well-planned vegetation planting can be an effective natural approach for river restoration.

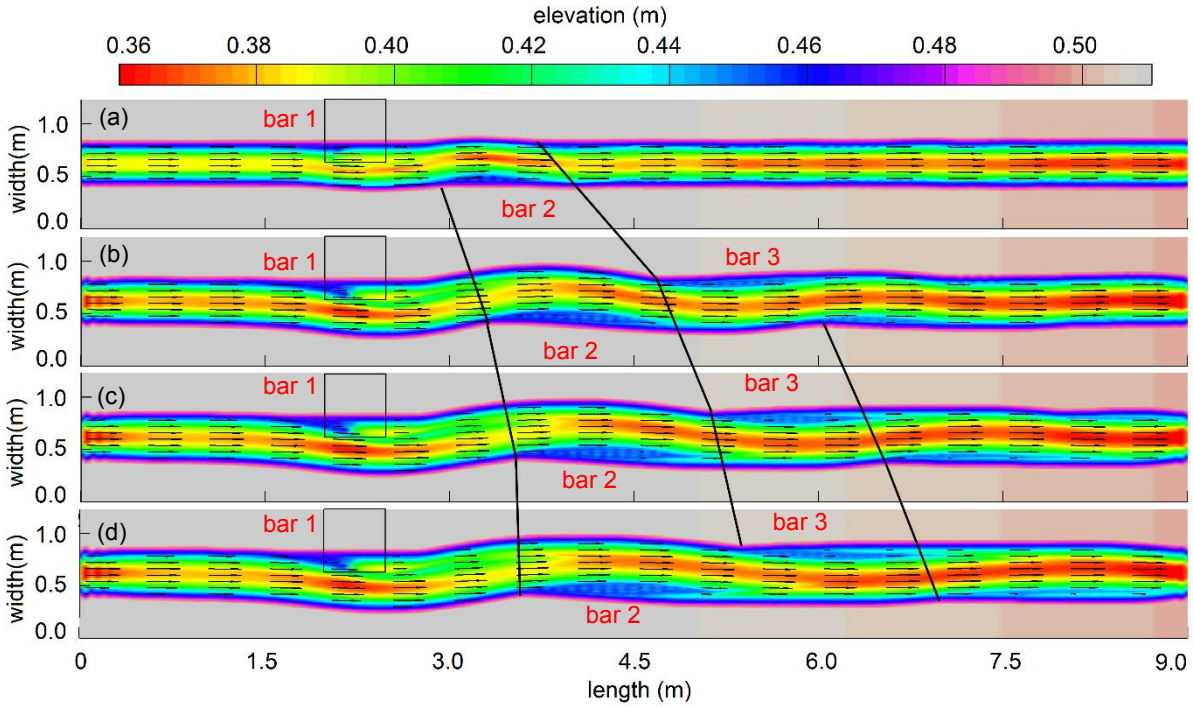

Figure 12. Channel pattern adjustment in response to a single vegetation zone under the condition of $1.5Q_{in}$

3.3. Morphological changes at a natural bend of River Creta

The capability and performance of the current model are further demonstrated and confirmed through application to a natural river reach. The study concerns a short reach of the River Greta located in Keswick, UK. The river reach is about 160 m long and has a varying width of 10 m to 40 m, featuring a sharp bend. The difficulty in modelling morphological changes in a natural bend has been investigated in details by Guan et al. (2016) which did not account for the effects of vegetation, Field surveys show that the river channel is extensively covered by riparian

463 vegetation that may be separated into two zones, i.e. the grass area at the outer bank and the
464 area at the inner bank of the river bend, as shown in Figure 13(a, b). During the flood periods,
465 morphological changes regularly take place at the sharp bend and field survey data is available
466 for this study.

467 Digital Terrain Models (DTMs) with a 1m × 1m resolution are reconstructed based on measured
468 raw point data to represent the bed terrain of the site in August 2005 and July 2006, before and
469 after the flooding period 2005-2006. The hydrograph of 15-minute intervals from January 2005 to
470 July 2006 (Figure 14) is available at the Low Briery station, upstream of the study site. Most of
471 the time, the flow discharge is smaller than 30 m^3/s. Field surveys demonstrate that
472 geomorphological changes are insignificant during the low flow period. Thus this study only
473 focuses on flooding periods when flow is greater than 30 m^3/s.

474 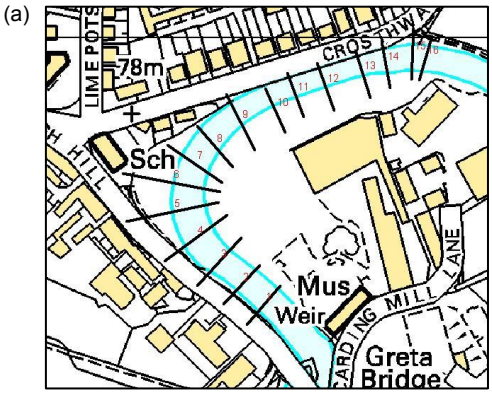

475 

476 Figure. 13 The study river reach: (a) map showing the study site; (b) photo facing upstream; (c) photo facing
477 downstream.

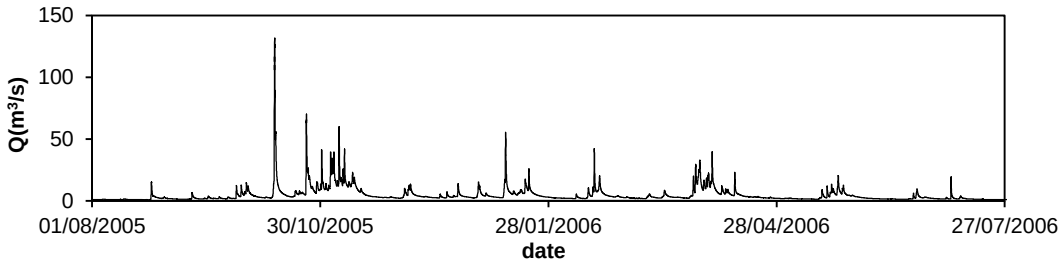

478

479 Figure 14. The inflow hydrograph recorded at the Low Briery gauge station

480 The study domain is discretised by a grid with uniform cells of 1m × 1m. The Manning's
481 coefficient is set to 0.03 in the river channel and 0.035 in the grass zone. The drag coefficient C_d
482 is assumed to be 2.0 for the emergent vegetation zone. The projected area λ is equal to 0.15 or
483 0.25 in order to test the model sensitivity. Non-uniform sediment with diameters of 0.02 m (30%),
484 0.04 m (40%), and 0.06 m (30%) is used and upstream inflow sediment load is neglected. The
485 recorded flow discharge is used as the inflow boundary condition to drive flow in the study reach,
486 and the corresponding stage-discharge curve is imposed at the outflow boundary. The radius of
487 the bend is estimated to be 60 m and used in the simulations.

488 Figure 15 shows the predicted and measured changes in bed elevation at the bend during the
489 multiple flood events from 2005 to 2006. Overall, the model predicts the formation of a bar, and
490 both the location and pattern of the deposition bar at the bend agree reasonably well with
491 measurements. Main deposition occurs at the inner bank of the bend. Small differences exist in
492 the projected area. The model predicts a similar magnitude in the deposition depth, compared
493 with the measured value. However, the model under-estimates the bar size; while in the main
494 channel, it over-estimates the bed erosion.

495 Due to the spatial and temporal complexity of a natural study case and the scarcity of high-
496 quality data, the simulation results are obtained without intensive model calibration. The
497 simulation results may also be affected by the following uncertain factors; The time interval
498 between the two DTMs representing the bed terrains before and after the flood is 1 year; the
499 current simulation only considers the flooding periods with flow rates over 30 m^3/s and the
500 recovery of channel morphology during low flow periods is neglected which inevitably leads to
501 uncertainty. Sediment flux from upstream may significantly affect the hydro-geomorphology in the
502 study reach but cannot be taken into account due to the lack of data. Moreover, accurate

parameterisation, such as sediment composition, viscosity and sediment transport capacity, is difficult, if not impossible, for a natural study case. Due to all these uncertainties linked to data scarcity, the simulation results are considered to be acceptable and the current model is demonstrated to be capable of predicting morphological changes during flooding over riparian vegetated channel in real cases.

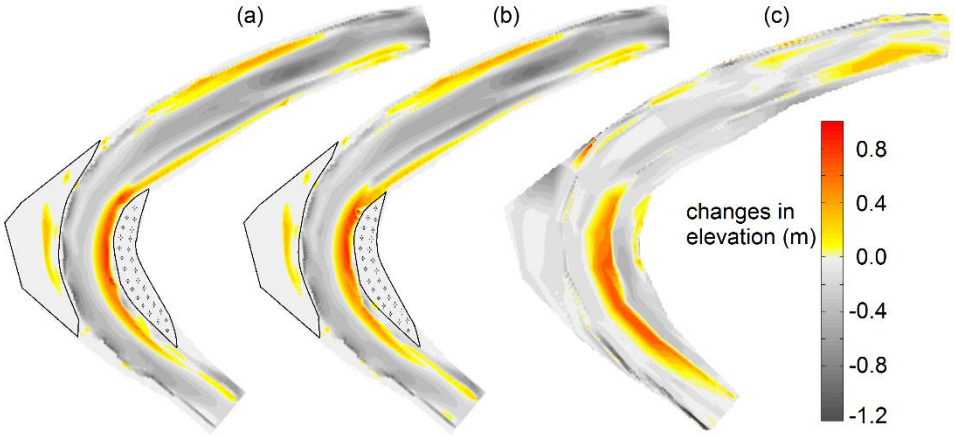

Figure 15. Predicted and measured changes in bed elevation during the flooding periods from August 2005 to July 2006: (a) λ = 0.15; (b) λ = 0.25; (c) the measured changes.

4. Conclusions

A two-dimensional model system has been developed and presented for simulating river hydraulics and morphology in the presence of various vegetation covers. The model system solves the full 2D shallow water equations and a non-equilibrium sediment transport equation, with a new module developed to consider the effects of both emergent and submerged vegetation. Also, the secondary flow effects have been incorporated into the 2D model system through the use of dispersion terms, leading to more accurate representation of river flow hydraulics.

The new model system has been validated against a number of laboratory-scale test cases, including flows over fixed and movable beds. The results show that both stream hydraulics and channel morphological changes in the presence of vegetation are reproduced reasonably well, with the bed elevation changes, bank retreat and thalweg meandering correctly captured. Numerical experiments are then designed and performed to investigate the adjustment of

channel patterns to riparian vegetation. Numerical predictions indicate that vegetation imposes significant influence on flow dynamics by pushing the flow towards the opposite sides of the vegetation zones, leading to excessive erosion. With multiple vegetation covers, the channel tends to adjust itself to the meandering form. More complicated and irregular vegetation covers may create diverse channel patterns, which may have important implications to biodiversity of the local environment. Finally, the model's performance and capability are further demonstrated by simulating a natural river bend and the simulation results indicate that the model is generally capable of predicting river hydraulics, sediment transport and morphological changes during flooding in a channel covered with vegetation. The model may therefore have great potential to be used for a variety of applications in river engineering and management.

Acknowledgements

The authors would like to thank colleague Samantha Mahaffey from Newcastle University for proof-reading the manuscript. Thanks also go to the Environment Agency for providing data for the River Creta case study, which may be requested from Inforequests.cmblnc@environment-agency.gov.uk.

References

Abad, J.D., Buscaglia, G.C., Garcia, M.H., 2008. 2D stream hydrodynamic, sediment transport and bed morphology model for engineering applications. Hydrological Processes 22(10) 1443-1459.

Alonso, C.V., 2004. Transport mechanics of stream-borne logs.

Anderson, B.G., Rutherfurd, I.D. and Western, A.W., 2006. An analysis of the influence of riparian vegetation on the propagation of flood waves. Environmental Modelling & Software, 21(9) 1290-1296.

Armanini, A., Cavedon, V., Righetti, M., 2010. Evaluation of the flow resistance in mobile bed vegetated rivers, In: Dittrich, K., Aberle & Geisenhainer (Ed.), River Flow 2010: Braunschweig, Gernany.

Baptist, M.J., Babovic, V., Uthurburu, J.R., Keijzer, M., Uittenbogaard, R.E., Mynett, A., Verwey, A.,

553 2007. On inducing equations for vegetation resistance. Journal of Hydraulic Research 45(4) 435-
554 450.
555 Begnudelli, L., Valiani, A., Sanders, B.F., 2010. A balanced treatment of secondary currents,
556 turbulence and dispersion in a depth-integrated hydrodynamic and bed deformation model for
557 channel bends. Advances in Water Resources 33(1) 17-33.
558 Bennett, S.J., Pirim, T., Barkdoll, B.D., 2002. Using simulated emergent vegetation to alter stream flow
559 direction within a straight experimental channel. Geomorphology 44(1–2) 115-126.
560 Bennett, S.J., Wu, W.M., Alonso, C.V., Wang, S.S.Y., 2008. Modeling fluvial response to in-stream
561 woody vegetation: implications for stream corridor restoration. Earth Surface Processes and
562 Landforms 33(6) 890-909.
563 Choi, S.-U., Kang, H., 2006. Numerical investigations of mean flow and turbulence structures of
564 partly-vegetated open-channel flows using the Reynolds stress model. Journal of Hydraulic
565 Research 44(2) 203-217.
566 Costabile, P. and Macchione, F., 2015. Enhancing river model set-up for 2-D dynamic flood modelling.
567 Environmental Modelling & Software, 67 89-107.
568 Cowan, W.L., 1956. Estimating hydraulic roughness coefficients. Agricultural Engineering(37) 473–
569 475.
570 Crosato, A., Saleh, M.S., 2011. Numerical study on the effects of floodplain vegetation on river
571 planform style. Earth Surface Processes and Landforms 36(6) 711-720.
572 Darby, S.E., 1999. Effect of riparian vegetation on flow resistance and flood potential. Journal of
573 Hydraulic Engineering-ASCE 125(5) 443-454.
574 De Vriend, H.J., 1977. A Mathematical Model Of Steady Flow In Curved Shallow Channels. Journal of
575 Hydraulic Research 15(1) 37-54.
576 Garcia, M.H., Lopez, F., Dunn, C., Alonso, C.V., 2004. Flow, turbulence, and resistance in a flume with
577 simulated vegetation.
578 Gorrick, S., Rodríguez, J.F., 2012. Sediment dynamics in a sand bed stream with riparian vegetation.
579 Water Resources Research 48(2).
580 Gran, K., Paola, C., 2001. Riparian vegetation controls on braided stream dynamics. Water
581 Resources Research 37(12) 3275-3283.
582 Green, J.C., 2005. Modelling flow resistance in vegetated streams: review and development of new

583 theory. Hydrological Processes 19(6) 1245-1259.
584 Guan, M., Wright, N., Sleigh, P., 2013. A robust 2D shallow water model for solving flow over complex
585 topography using homogenous flux method. International Journal for Numerical Methods in Fluids
586 73(3) 225-249.
587 Guan, M., Wright, N., Sleigh, P., 2014. 2D Process based morphodynamic model for flooding by
588 noncohesive dyke breach. Journal of Hydraulic Engineering 140(7).
589 Guan, M., Wright, N., Sleigh, P., 2015a. Multimode morphodynamic model for sediment-laden flows
590 and geomorphic impacts. Journal of Hydraulic Engineering 141(6).
591 Guan, M., Wright, N.G., Sleigh, P.A., Carrivick, J.L., 2015b. Assessment of hydro-morphodynamic
592 modelling and geomorphological impacts of a sediment-charged jökulhlaup, at Sólheimajökull,
593 Iceland. Journal of Hydrology 530 336-349.
594 Guan, M., Wright, N.G., Sleigh, P.A., Ahilan, S. and Lamb, R., 2016. Physical complexity to model
595 morphological changes at a natural channel bend, Water Resources Research 52 6348–6364.
596 Guymer, I., 1998. Longitudinal Dispersion in Sinuous Channel with Changes in Shape. Journal of
597 Hydraulic Engineering 124(1) 33-40.
598 Hickin, E.J., 1984. Vegetation and river channel dynamics. Canadian Geographer-Geographe
599 Canadien 28(2) 111-126.
600 Hupp, C.R., Osterkamp, W.R., 1996. Riparian vegetation and fluvial geomorphic processes.
601 Geomorphology 14(4) 277-295.
602 Hou, J., Liang, Q., Zhang, H. and Hinkelmann, R., 2015. An efficient unstructured MUSCL scheme for
603 solving the 2D shallow water equations. Environmental Modelling & Software, 66 131-152.
604 James, C.S., Birkhead, A.L., Jordanova, A.A., O'Sullivan, J.J., 2004. Flow resistance of emergent
605 vegetation. Journal of Hydraulic Research 42(4) 390-398.
606 Jang, C.L., Shimizu, Y., 2007. Vegetation effects on the morphological behavior of alluvial channels.
607 Journal of Hydraulic Research 45(6) 763-772.
608 Jordanova, A.A., James, C.S., 2003. Experimental study of bed load transport through emergent
609 vegetation. Journal of Hydraulic Engineering-ASCE 129(6) 474-478.
610 Keller, E.A., Swanson, F.J., 1979. Effects of large organic material on channel form and fluvial
611 processes. Earth Surface Processes and Landforms 4(4) 361-380.
612 Li, S.S., Millar, R.G., 2011. A two-dimensional morphodynamic model of gravel-bed river with

floodplain vegetation. Earth Surface Processes and Landforms 36(2) 190-202.

Liang, Q.H., 2010. Flood Simulation Using a Well-Balanced Shallow Flow Model. Journal of Hydraulic Engineering-ASCE 136(9) 669-675.

Lien, H., Hsieh, T., Yang, J., Yeh, K., 1999. Bend-Flow Simulation Using 2D Depth-Averaged Model. Journal of Hydraulic Engineering 125(10) 1097-1108.

Lopez, F., Garcia, M.H., 2001. Mean flow and turbulence structure of open-channel flow through non-emergent vegetation. Journal of Hydraulic Engineering-ASCE 127(5) 392-402.

Meyer-Peter, E., Müller, R., 1948. Formulas for bed load transport, Proc., 2nd Meeting: Stockholm, Sweden, pp. 39–64.

Morin, J., Leclerc, M., Secretan, Y., Boudreau, P., 2000. Integrated two-dimensional macrophytes-hydrodynamic modeling. Journal of Hydraulic Research 38(3) 163-172.

Odgaard, A., 1986. Meander Flow Model. I: Development. Journal of Hydraulic Engineering 112(12) 1117-1135.

Pasche, E., Rouvé, G., 1985. Overbank flow with vegetatively roughened floodplains. Journal of Hydraulic Engineering 111(9) 1262-1278.

Sellin, R.H.J., Bryant, T.B., Loveless, J.H., 2003. An improved method for roughening floodplains on physical river models. Journal of Hydraulic Research 41(1) 3-14.

Song, C.G., Seo, I.W., Kim, Y.D., 2012. Analysis of secondary current effect in the modeling of shallow flow in open channels. Advances in Water Resources 41(0) 29-48.

Soulsby, R., 1997. Dynamics of marine sands: a manual for practical applications. Thomas Telford, London, UK.

Stone, B.M., Shen, H.T., 2002. Hydraulic resistance of flow in channels with cylindrical roughness. Journal of Hydraulic Engineering-ASCE 128(5) 500-506.

Tal, M., Paola, C., 2007. Dynamic single-thread channels maintained by the interaction of flow and vegetation. Geology 35(4) 347-350.

Tal, M., Paola, C., 2010. Effects of vegetation on channel morphodynamics: results and insights from laboratory experiments. Earth Surface Processes and Landforms 35(9) 1014-1028.

Temple, D.M., 1986. Velocity distribution coefficients for grass-lined channels. Journal of Hydraulic Engineering-ASCE 112(3) 193-205.

Tsujimoto, T., 1999. Fluvial processes in streams with vegetation. Journal of Hydraulic Research 37(6)

789-803.

Vacondio, R., Dal Palù, A. and Mignosa, P., 2014. GPU-enhanced Finite Volume Shallow Water solver for fast flood simulations. Environmental Modelling & Software, 57 60-75.

Vionnet, C.A., Tassi, P.A., Martin Vide, J.P., 2004. Estimates of flow resistance and eddy viscosity coefficients for 2D modelling on vegetated floodplains. Hydrological Processes 18(15) 2907-2926.

Wu, F.C., Shen, H.W., Chou, Y.J., 1999. Variation of roughness coefficients for unsubmerged and submerged vegetation. Journal of Hydraulic Engineering-ASCE 125(9) 934-942.

Wu, W., 2004. Depth-averaged two-dimensional numerical modeling of unsteady flow and nonuniform sediment transport in open channels. Journal of Hydraulic Engineering-ASCE 130(10) 1013-1024.

Wu, W., Shields, F.D., Bennett, S.J., Wang, S.S.Y., 2005a. A depth-averaged two-dimensional model for flow, sediment transport, and bed topography in curved channels with riparian vegetation. Water Resources Research 41(3) W03015.

Wu, W.M., Shields, F.D., Bennett, S.J., Wang, S.S.Y., 2005b. A depth-averaged two-dimensional model for flow, sediment transport, and bed topography in curved channels with riparian vegetation. Water Resources Research 41(3).